JMEPEG (2021) 30:1768–1779
https://doi.org/10.1007/s11665-021-05490-0

1059-9495/$19.00

Plasma-Sprayed Hydroxyapatite-Strontium Coating for Improved Corrosion Resistance and Surface Properties of Biodegradable AZ31 Mg Alloy for Biomedical Applications

Puneet Bansal, Gurpreet Singh, and Hazoor Singh Sidhu

Submitted: 15 August 2020 / Revised: 17 December 2020 / Accepted: 11 January 2021 / Published online: 29 January 2021

Magnesium and its alloys have been introduced as innovative orthopedic implants due to their potential in serving lightweight, bio-active, degradable, and biocompatible properties. Mg and its alloys corrode rapidly in a biological environment and result in losing mechanical properties. However, to enhance corrosion resistance and mechanical properties, Mg alloy was plasma-sprayed with pure hydroxyapatite (HA) and HA-reinforced with strontium (Sr) powder at three levels (4, 8, and 12 wt.%). Surface parameters such as microhardness, surface roughness, and wettability were examined. The electrochemical technique was used to study the corrosion behavior in Ringer's solution. The outcomes confirmed that with the rise in Sr content in pure HA coatings, the surface properties as well as the corrosion resistance improved significantly. The contact angle of substrates under examination exhibits hydrophilic nature. Collectively, the findings of this study signify HA/Sr reinforced coatings are a promising approach to improve surface properties and corrosion behavior of Mg alloys for future bone implant applications.

Keywords coating, hydroxyapatite, magnesium alloys, plasma spray, strontium

1. Introduction

Metallic biomaterials such as stainless steel, cobalt alloys, and titanium-based alloys have performed a significant role in biomedical applications, like in the orthopedic and dentistry field due to high mechanical strength and load-bearing properties (Ref 1, 2). These metallic alloys are non-biodegradable in the biological environment (Ref 3). The wear and corrosion debris in these alloys increase the chances of infection in the surrounding environment (Ref 4). Moreover, these non-degradable implants mismatch the mechanical properties of natural tissues and result in harmful effects after implantation (Ref 5, 6).

In recent years, the biodegradable materials like polymers and ceramics gain a huge interest in the biomedical field and termed as an innovative replacement over non-biodegradable materials. On the other hands, magnesium alloys are considered a promising biomaterial, because of the desirable properties as they are biodegradable and possess the lightweight and an excellent strength-to-weight ratio (Ref 7, 8). In addition to this, the yield strength along with the elastic modulus is nearly similar to the human bone (Ref 9). However, the magnesium alloys corrode very quickly in physiological surroundings that result in the formation of a corrosive layer which is generally constituted of magnesium hydroxide as well as gaseous hydrogen is released (Ref 10). This degradation leads to the weakening of its mechanical integrity, and therefore, the inserted bio-implants are not able to handle the exerted load, which in the end triggers implant failure (Ref 11). In order to slow down the quick degradation of Mg alloys and to maintain the proper mechanical stability during implantation different modification techniques are applied that include bio-ceramic coatings as well as surface grafting (Ref 12).

Hydroxyapatite coatings on Mg substrates were the best approach among all the methods (Ref 13, 14). In the biological conditions, hydroxyapatite works as a protective barrier against metal ions being released from the substrate. HA has several chemical and biological similarities to a human bone (Ref 15, 16). These coatings promote the growth of bone cells and advance the contact among body tissue and coated substrates (Ref 17, 18). Different methods were used to deposit coatings on the substrates, such as sol–gel coatings, RF magnetron sputtering, electrochemical depositions, and thermal spray, respectively (Ref 19-21). Among all these coating methods, plasma spraying is a simple process that has a superior deposition efficiency, including a broad variety of particle sizes. Only plasma spray methodology was approved by the Food and Drug Administration (FDA), the USA for coating bio-implants (Ref 22, 23).

In HA coatings, the addition of reinforcement powders such as CNTs, Sr, Zn, SiO_2, and CaP are found to enhance the hardness and corrosion resistance (Ref 24-26). Strontium incorporation in HA coatings advances osteoblast as well as osteoclast activity, which results in bone development of apatite film on the coatings (Ref 27, 28). As per the available literature, a limited study is performed on plasma-sprayed HA/Sr reinforced coating on AZ31 alloys for biomedical applications.

Puneet Bansal and **Gurpreet Singh**, Department of Mechanical Engineering, Punjabi University, Patiala, Punjab 147002, India; and **Hazoor Singh Sidhu**, Yadavindra College of Engineering, Punjabi University G.K. Campus, Talwandi Sabo, Punjab 151302, India. Contact e-mail: gurpreetsnabha@yahoo.com.

Therefore, in this article, electrochemical corrosion behavior, as well as the surface properties of AZ31 alloy, was examined.

2. Materials and Methods

2.1 Samples Preparation and Coating Deposition

Magnesium alloy (AZ31), containing (wt.%) (Mg 95.998, Al 2.83, Zn 0.80, Mn 0.37, and Cu 0.002) was cut to (15×10×5) mm rectangular substrates. Spray powders of HA and Sr were supplied by Medicoat, Etupes, France, and Nano Labs, India, respectively. The plasma gun MF4 at Metallizing Equipment, Jodhpur, India was utilized to produce pure HA, HA-reinforced with Sr coatings (4 wt.%, 8 wt.%, and 12 wt.%) at three levels on AZ31 alloy. The spraying parameters were arc current of 600 A with 57 V of arc voltage. Argon and hydrogen were selected as primary and secondary gas at 38.5 SLPM and 5 SLPM. The spraying gap of 75 mm was maintained between both plasma gun and substrate at a powder flow rate of 9 standard liter per minute (SLPM).

2.2 Characterization

XRD analysis (X'Pert Pro Panalytical Pw-3050/60, the Netherlands) was used to perform the structural characterization with Cu-Ka radiation (k = 0.154059 nm) over 20°-60° (2θ) range. Scanning electron microscope (SEM: JEOL JSM-6510LV, Akishima, Japan) equipped with energy- dispersive x-ray spectroscopy (EDX) was utilized for the microstructural and compositional analyses of the coated samples before and after corrosion testing in Ringer's solution and operated at 13 keV all the samples. The SEM examination of the experimental substrates was also carried out from the cross-sections. The specimens were cut across the cross-section with a precise low-speed saw then mounted in epoxy resin. The substrates were buffed with 220-2000 grade emery sheets to achieve a mirror finish. Prior to SEM/EDX analysis to attain the required conductivity, the samples were covered using a thin layer of gold sputtering.

2.3 Surface Properties

The microhardness from the polished cross-section was analyzed via microhardness tester (Wolpert Wilson 402MVD, Germany) by applying a load of 50 gf and dwell time 15s. To a obtain polished cross-section, the samples were firstly cut across the cross-section using a low-speed precision sectioning saw and then mounted in epoxy resin. Subsequently, the polishing of the samples was performed with emery papers up to grade 2000. Finally, alumina slurry was used for buffing of the samples on a napped cloth. Surface roughness tester (Mitutoyo SJ-210, Kamasaki, Japan) having measuring force and stylus tip of 75 mN and 2 mμR at 60° was engaged to measure the surface roughness. Surface wettability was determined from the contact angle measurement using a goniometer (First Ten Angstroms FTA2000, the USA) having surface tension (±0.1 mN/m), drop volume (±1.0 μl), and drop radius (± 0.05 mm). The Ringer's solution was used for contact angle measurements. The surface properties' measurements were performed in triplicate on five samples from each group. The average ± standard deviation of all the measurements is reported in the present study.

2.4 Corrosion Behavior

The corrosion behavior was examined by potentiodynamic polarization in Ringer's solution at pH 7.2. The electrochemical measurements were attained by means of Gamry Potentiostat/Galvanostat/ZRA (G-750) using a typical cell of three-electrode arrangements. AgCl and graphite rod served as reference and counter electrodes, respectively, while the uncoated/coated sample formed the working electrode. The potentiodynamic scan was performed from an initial potential of −0.25 V to the final potential of 0.25 V with respect to the open-circuit potential at a scan rate of 0.5 mV/s. The potentiodynamic curve was then analyzed with Echem Analyst Software (Gamry Instruments, Warminster, the USA) to acquire the values of electrochemical parameters by using Tafel extrapolation. Before corrosion testing, the substrates were dipped in the Ringer's solution, while 1 cm^2 area was uncovered and all remaining sides are polished using epoxy resin. For each group of samples, three measurements were determined by performing the corrosion analyses with five replicates.

2.5 Weight Loss Testing

The weighting scale of Kern ABS 220-4N Series, Europe with least count of 0.01 mg and operating temperature 5-40° C was used for weight loss testing. For 3 weeks, the immersion testing was performed in Ringer's solution. The substrates were soaked in separate containers and each retained a 30 ml solution. The samples were removed from the containers after 7, 14, and 21 days and then rinsed with deionized water (DI). The substrates were first inserted in the chromic acid over 10 min to remove the corrosion components and then cleaned by DI water. The weight loss method was applied to measure the corrosion level. The relation (DR = W/At) helps to calculate the degradation rate (DR) (mg cm^{-2} d^{-1}), W defines the substrate weight loss, A and t denote the surface area (cm^2) and exposure time (days), respectively (Ref 29, 30).

3. Results and Discussion

SEM was introduced to study the microstructure of both the spraying powders as shown in Fig. 1(a) and (b). HA particles show spherical, while Sr particles reveal irregular appearance. In Fig. 2, x-ray diffraction patterns of HA as well as HA/Sr reinforced powders are shown. The peaks strength associated with Sr improves as the Sr content rises in HA. As revealed from the figure, the diffraction patterns did not exhibit any changes in position when the two powders were mixed. To match the peaks of pure HA and Sr powders, the JCPDS cards (004-932) and (0-001-0574) were employed which are deeply evident with the cards (Ref 31-33).

Figure 3 demonstrates the XRD characteristics of HA and HA-reinforced coatings formed on plasma-sprayed substrates. HA remained the primary phase in all the coatings. Along with the primary HA phase, other calcium phosphate phases were also detected such as amorphous calcium phosphates (ACP) peaks, namely α-tricalcium phosphate (α-TCP), β-tricalcium phosphate (β-TCP) as well as tetracalcium phosphate (TTCP) matched by JCPDS card 9-169, 25-1137, as well as 9-348. The appearance of ACP, TCP, and TTCP is related to chemical degradation of the HA which is understood as the result of a dihydroxylation of the compound. The presence of ACP is

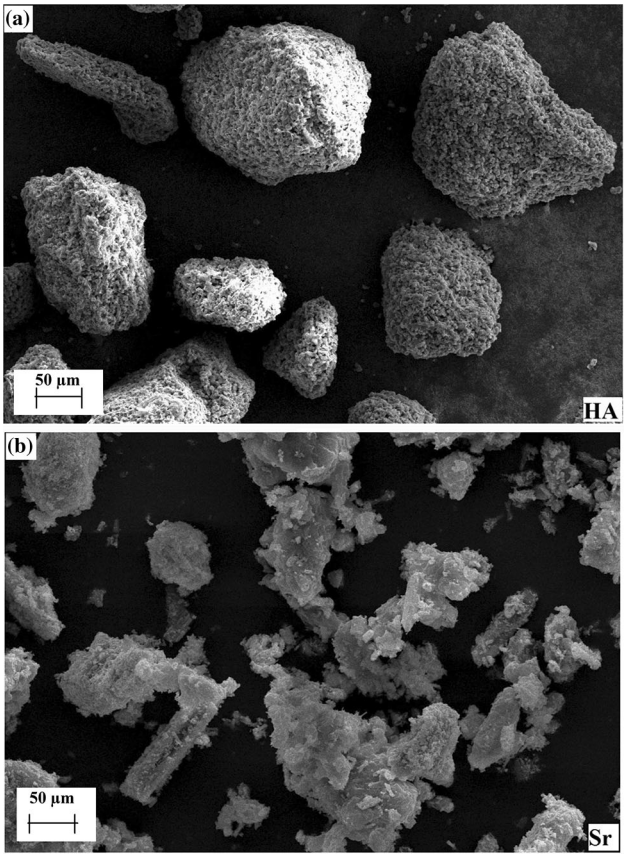

Fig. 1 SEM micrograph of (a) HA and (b) Sr powder

beneficial for the early bio integration of the implants (Ref 34). The peaks corresponding to ACP are reduced upon increasing Sr content in HA (Ref 35). The difference in the thermal conductivity of both the powders could be a promising reason for the lowering of the amorphous phase. The thermal conductivity of strontium powder is very high (35 W/m K) and nearly 50 times as compared to that of hydroxyapatite (0.7 W/m K) (Ref 36). It results in the development of a thermal gradient around the boundary of the HA/Sr and causes a decrease in the cooling rate of the neighboring HA-region (Ref 37).

As shown in Fig. 4(a), SEM image of the substrate, plasma-sprayed with hydroxyapatite, ensures the throughout domination of spheriodized particles in comparison to lesser accumulated splats. In reinforced coating {Fig. 4(b), (c), and (d)} with rising Sr content in HA lesser spheroidized particles are noticed and majorly well-flattened splats have appeared on the surface. The variation is because of the dissimilarity of thermal conductivity in hydroxyapatite and strontium powders. The lack of partially melted/unmelted crystals and the appearance of well-flattened splats suggest the powders have been properly melted and sprayed. On the other hands, no major cracks exist at the coated surfaces. The development of microcracks in the coating may lead to quick degradation of the sample as well as the coating failure because of delamination, as it promotes direct interaction among the coated sample and the body fluids (Ref 38, 39). The EDX analysis has been used to analyze the atomic composition of the coating. The obtained Ca/P ratio for the HA-coated sample was 1.73 and reduced to the range of 1.72, 1.71, and 1.69 after reinforcement, when the content of Sr continues to increase. The Ca/P ratio between 1.67–1.76 was

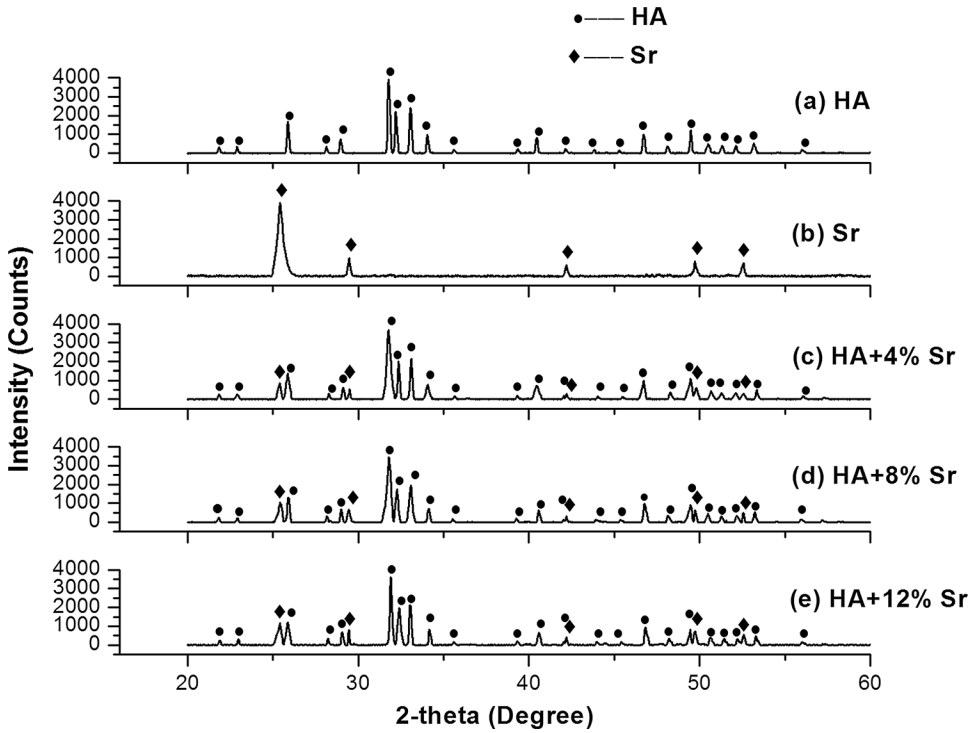

Fig. 2 XRD patterns of (a) HA, (b) Sr, (c) HA + 4%Sr, (d) HA + 8%Sr, and (e) HA + 12%Sr powders

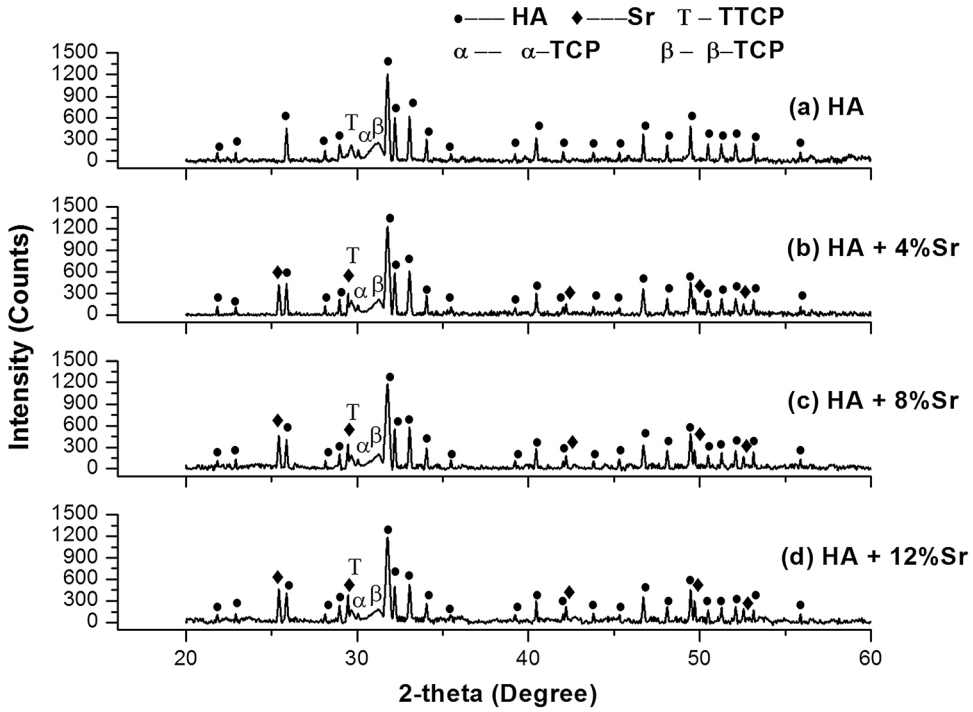

Fig. 3 XRD patterns of plasma-sprayed coatings on AZ31 alloy (a) HA, (b) HA + 4%Sr, (c) HA + 8%Sr, and (d) HA + 12%Sr

termed as a standard ratio for bio-implants coated with HA (Ref 40, 41).

Figure 5 signifies the cross-section images of the coated samples. The average thickness obtained for the coating was 120 μm. The region referred to 'S,' 'C,' and 'E' in the cross-sectional descriptions symbolizes the substrate, coated surface, as well as, the epoxy resin. Crack-free coatings were obtained for all the samples on the interface. HA coatings revealed a prolonged as well as defect-free substrate interaction. Similarly, the HA-reinforced coatings appeared well-bonded to the substrate as no empty asperities were noticed across the interface. No bearings from the sample were shifted to coatings and similarly, no component moved from coating to sample. This can be concluded that the impacted molten substance had shown perfect adherence to the AZ31 sample surface resulting in good metallurgical bonding (Ref 42).

3.1 Analysis of Surface Properties

The outcomes of the microhardness evaluations of samples are shown in Fig. 6. The surface hardness assumes a significant part in defining the superiority of a coating (Ref 43, 44). HA + 12%Sr-coated substrate exhibits a higher hardness value (288 ± 4) HV as compared to all the coated samples. The obtained values indicate the increase in microhardness on increasing Sr content in pure HA. The generation of the layered framework by the uniform distribution of reinforced Sr particles could be the reason for the increment in the surface hardness value for reinforced HA coatings. The earlier experiments carried out suggested that HA-reinforced coated substrates retained greater surface hardness in comparison to pure HA coating. According to the literature, the harder the surface, the higher the corrosion wear resistance, since it pauses a fast deterioration of the coated substrate (Ref 45, 46).

Figure 7 illustrates the mean value of surface roughness. HA + 12%Sr-coated AZ31 substrate retains the lowest surface roughness with R_a = (4.3 ± 0.03 μm). In addition to this, HA-coated sample attains the maximum roughness with R_a = (5.2 ± 0.04 μm). It was noticed that the surface roughness decreases on the continuing addition of strontium powder (Ref 47). The SEM micrographs (Fig. 4) revealed a comparatively flattened surface including reduced melt-resolidified particles as the amount of Sr powder raised in HA. As previously discussed, it reduces the solidification rate, caused by the difference in thermal conductivity of HA and Sr. The investigations performed to observe the influence of surface roughness on bio-implants indicated that significantly rough surface results in proper incorporation of protein in bio-implant's surface. This in turn caused adherence of cell/tissue with the bio-implant in a better way (Ref 48, 49). The surface roughness values attained in the present study are inside the range (R_a = 2–6 μm) generated by plasma-sprayed coatings (Ref 50).

The substrates were tested for wettability to explain hydrophilic and hydrophobic behavior. The contact angles of the exposed surface are presented in Fig. 8. The obtained results indicate that bare AZ31 reveals a hydrophobic surface having a contact angle of (90.07° ± 3); however, hydrophilic nature was found for all the coated samples. On reinforcement of Sr, the rise in contact angle value was recorded. The angle below 60° reveals hydrophilic nature, and the hydrophilic surface ensures better cell attachment in comparison to a hydrophobic surface (Ref 51, 52).

3.2 Electrochemical Testing

To investigate the corrosion performance of the AZ31 samples, the Tafel extrapolation approach was applied. The potentiodynamic curves of all the samples are shown in Fig. 9. In the valuation and comparison of corrosion behavior, the crucial parameters are corrosion potential (E_{Corr}) as well as corrosion current density (I_{Corr}) summarized in Table 1. The outcomes showed the I_{Corr} (250 ± 5 μA) of bare AZ31 alloy

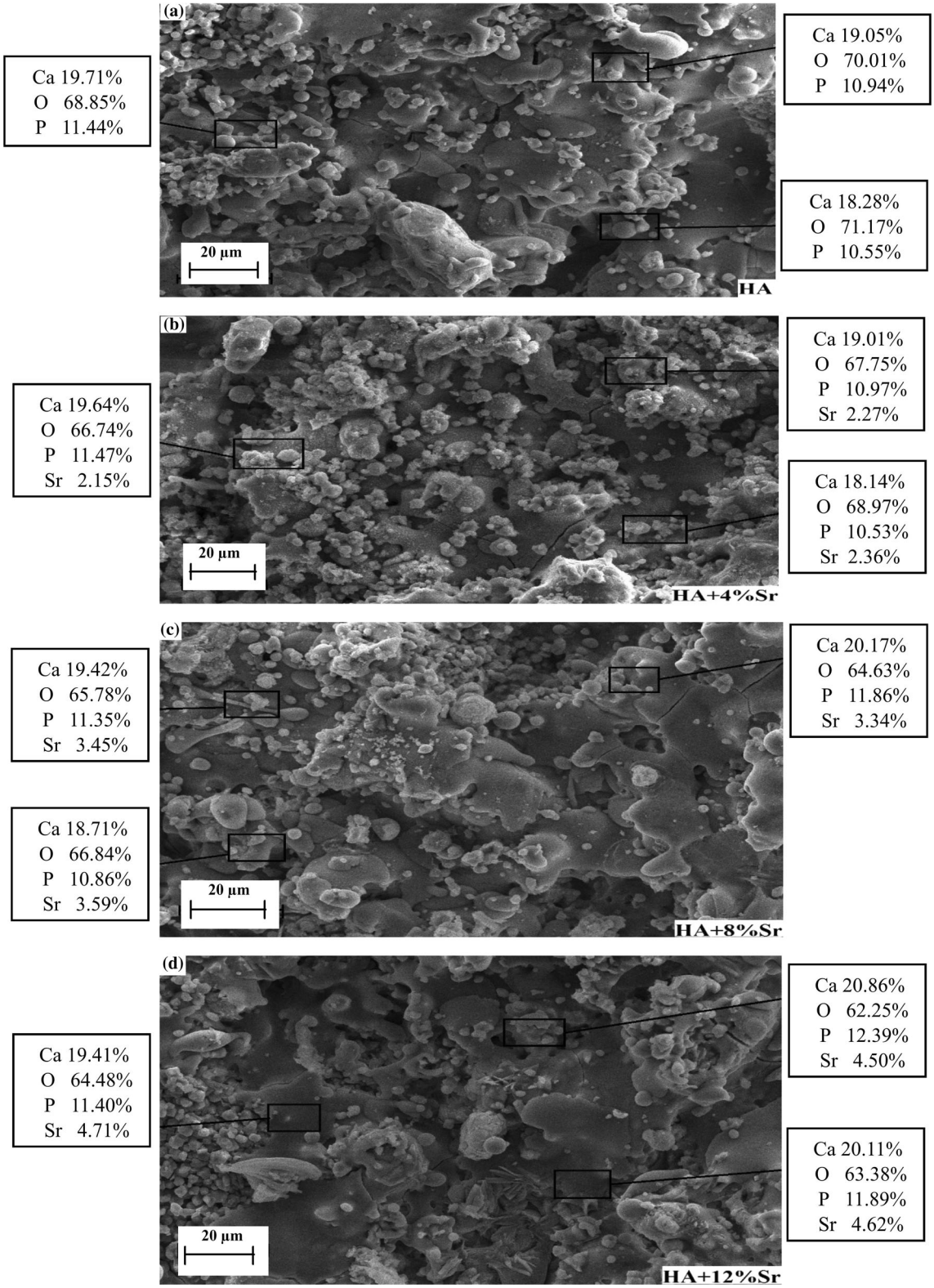

Fig. 4 SEM images and EDS analysis of plasma-sprayed coatings (a) HA, (b) HA + 4%Sr, (c) HA + 8%Sr, and (d) HA + 12%Sr

was the highest; however, HA + 12%Sr-coated AZ31 substrate attained the lowest I_{Corr} (37.6 ± 3 µA). The E_{Corr} of coated samples was nobler as compared to bare AZ31 alloy. With rising Sr reinforcement in HA coatings, it was observed that the maximum corrosion resistance was obtained for HA + 12%Sr-coated substrate. For HA reinforcement coatings, similar outcomes of improved resistant to corrosion are noticed (Ref 53, 54). Enhanced corrosion resistance, as stated in prior studies, promotes lifelong implant-tissue bonding in a lesser amount of time and facilitates the fast healing of destroyed

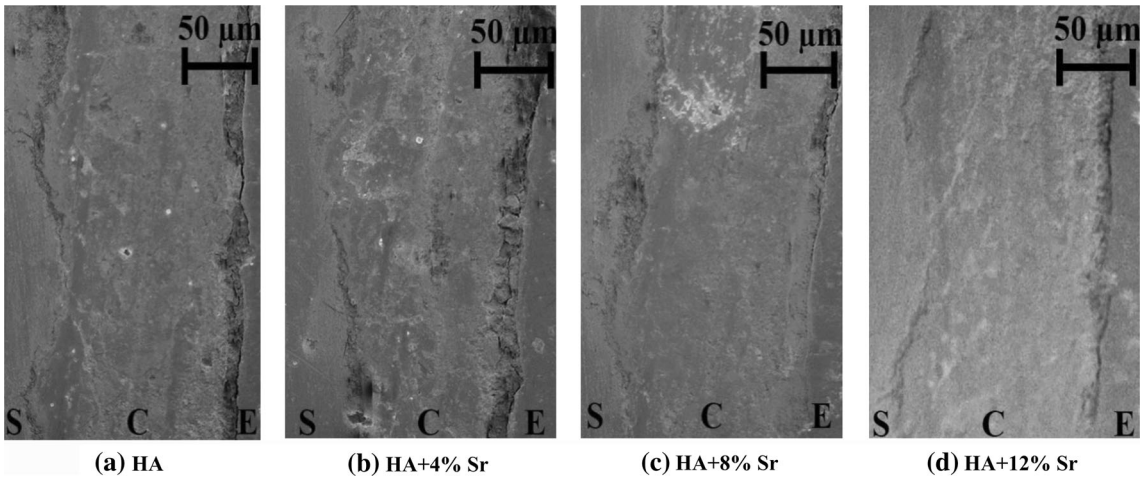

Fig. 5 SEM images of plasma-sprayed coatings from cross-section (a) HA, (b) HA + 4%Sr, (c) HA + 8%Sr, and (d) HA + 12%Sr

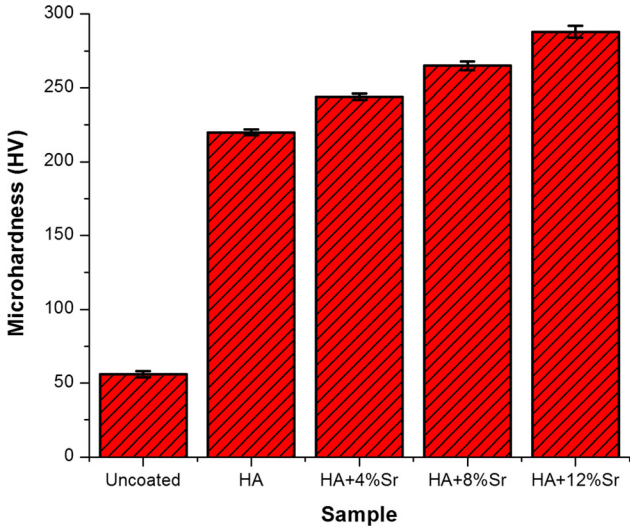

Fig. 6 Microhardness of different samples

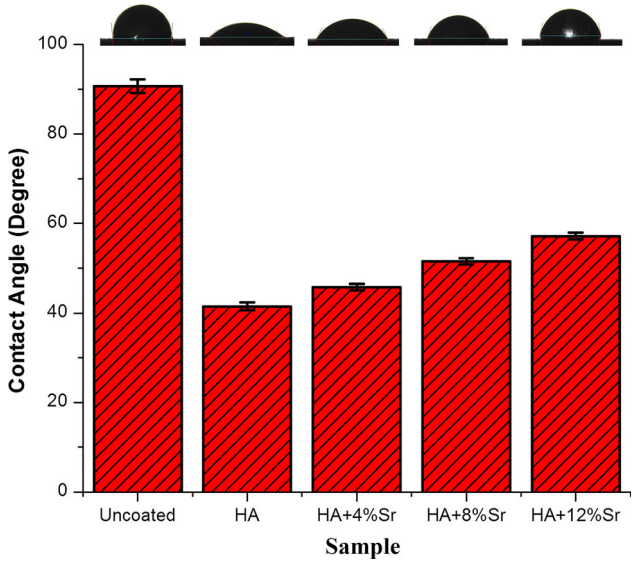

Fig. 8 Contact angle and droplet outline of different samples

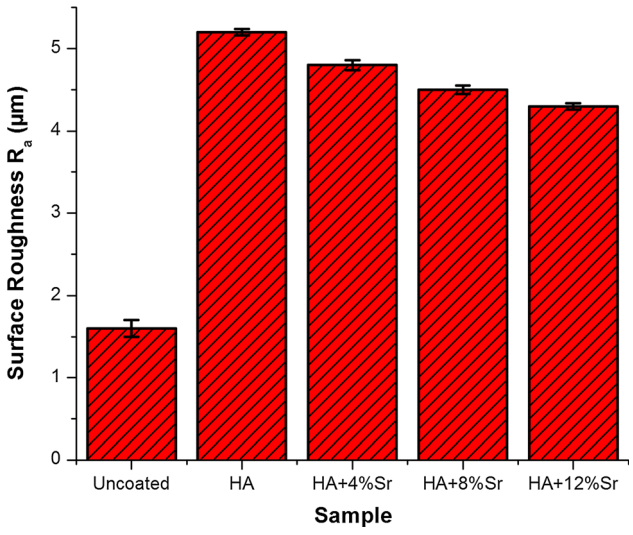

Fig. 7 Surface roughness of different samples

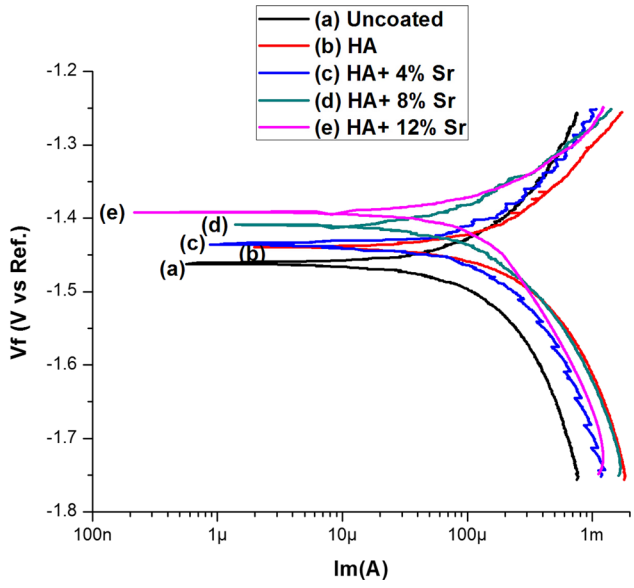

Fig. 9 Potentiodynamic polarization curves

tissue. Greater corrosion resistance gives rise to the development of stronger implant-tissue attachment. In addition to this, it leads to swift healing of the damaged tissue and in a short time interval (Ref 55).

The findings of the electrochemical analysis indicate that the fortified HA/Sr coatings revealed a greater protective role against corrosion of the AZ31 alloy in comparison to pure HA coatings. With rising the Sr amount in HA, the I_{Corr} value goes on decreasing. In previous investigations, it was also disclosed that HA/Sr-coated samples showed significantly greater resistance to corrosion compared to uncoated substrates (Ref 56, 57). The ions arising due to corrosion in metallic implants can influence cell metabolism, i.e., corrosion current can affect cell behavior (Ref 58).

In this report, the variation between the roughness outcomes may describe the decline in I_{Corr} value. This is a significant parameter that affects a surface's corrosion behavior. A rough surface is more prone to pit formation than the smoother one. It gives rise to pitting corrosion that reduces the protection ability of that surface (Ref 59). The previous researchers also clarified that the increase in surface roughness is directly related to its decreased corrosion resistance. The higher corrosion resistance inhibits the rapid corrosion of Mg implants upon implantation that leads to the retention of mechanical strength of the coated substrate (Ref 60, 61). In the present work, with the rise of the Sr amount in pure HA, the value of surface roughness declines that results in improved corrosion resistance.

Table 1. Mean values (standard deviation) of potentiodynamic polarization parameters of uncoated and coated AZ31 alloy in Ringer's solution

Sample	E_{Corr}, V	I_{Corr}, μA/cm^2	β_a, e^{-3} V/decade	β_c, e^{-3} V/decade
Uncoated	− 1.46 ± 0.005	250 ± 5	361.7	529.9
HA	− 1.44 ± 0.006	150 ± 3	115.7	145.4
HA + 4%Sr	− 1.43 ± 0.005	94.9 ± 4	131.5	171.8
HA + 8%Sr	− 1.41 ± 0.005	67.6 ± 3	90.0	96.5
HA + 12%Sr	− 1.39 ± 0.004	37.6 ± 3	39.0	52.0

After implantation, the implants interact in a physiological environment that is delicate but hostile at the same time. Therefore, in addition to favorable biological properties, biomaterials should also possess adequate mechanical strength. Surface hardness, a key mechanical property, can be used for the assessment of functional effectiveness as well as the quality of coating (Ref 62, 63). In this research work, the surface microhardness tends to increase on rising Sr reinforcement and HA + 12%Sr coatings achieved the maximum value. The high hardness of the surface enhances the biomechanical compatibility of the metallic implant by facilitating good wear resistance in vivo and improving the long-term survivability. Moreover, coatings with higher hardness impart high load-carrying capacity to metallic implants (Ref 64).

The XRD patterns of all samples after immersion are represented in Fig. 10. The existence of all major phases was observed in the as-deposited coatings, and no other phase development was noticed, therefore, the phase purity was retained by the coating even after immersion. The overall intensity of the peaks improved marginally. In vivo tests, both the properties, microstructure as well as phase purity affects the biological reaction of hydroxyapatite-coated samples. This

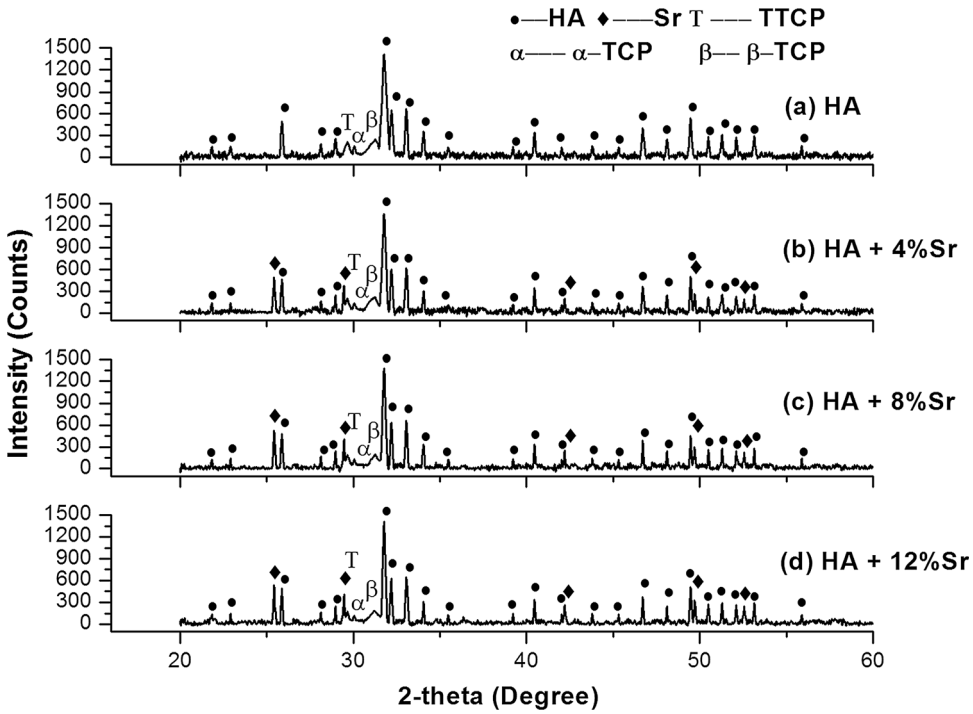

Fig. 10 XRD patterns of plasma-sprayed coatings after corrosion testing on AZ31 alloy (a) HA, (b) HA + 4%Sr, (c) HA + 8%Sr, and (d) HA + 12%Sr

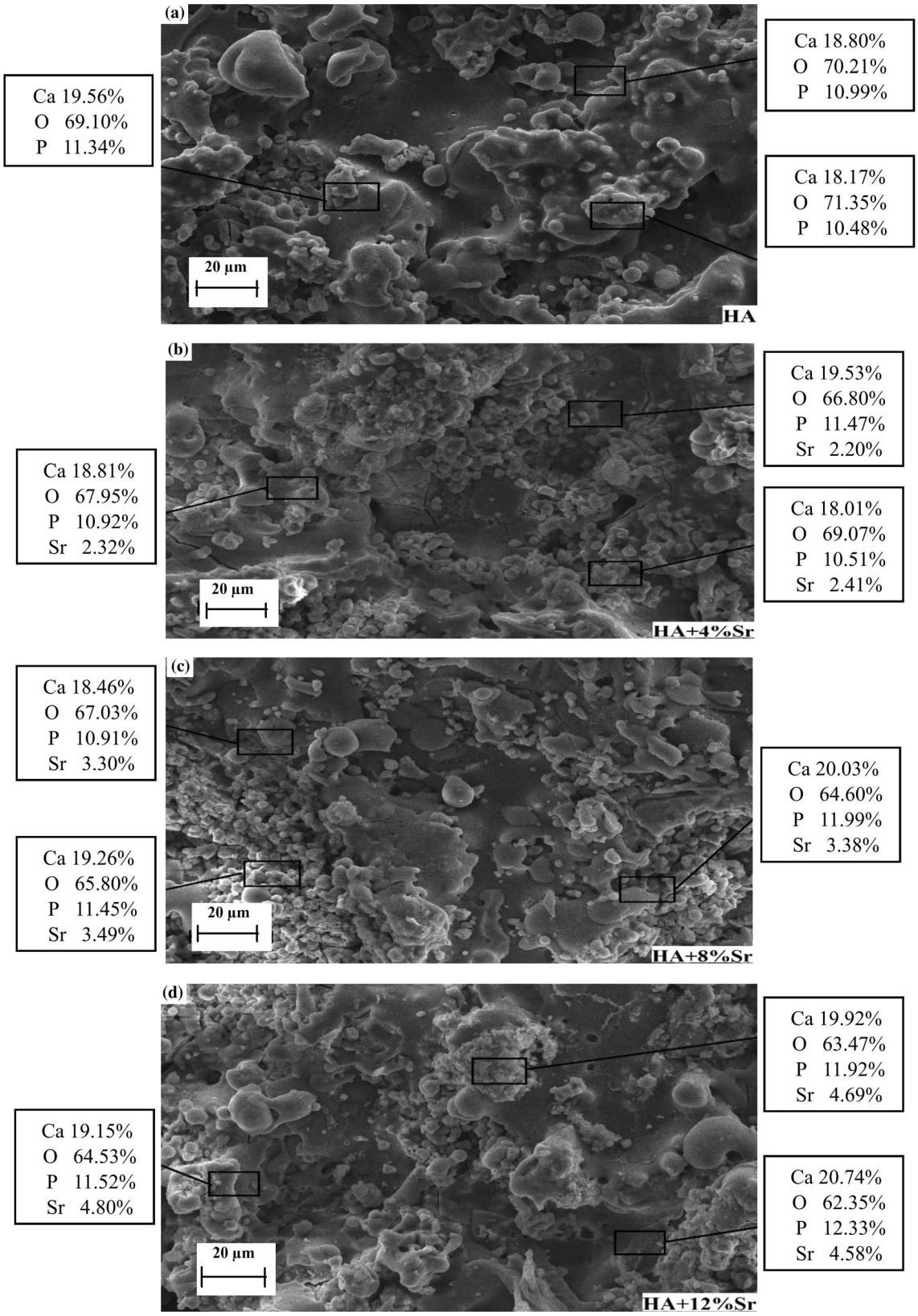

Fig. 11 SEM Images and EDS of plasma spray coatings after corrosion testing (a) HA, (b) HA + 4%Sr, (c) HA + 8%Sr, and (d) HA + 12%Sr

leads to accelerate bone growth and also results in a longer lifetime of the implant (Ref 65, 66).

SEM and EDS examinations were applied after the corrosion analysis of all the substrates. As seen from Fig. 11, micrographs of HA coatings remain unchanged, and no visible cracks have been found on all the coated substrates after immersion. In as-sprayed coatings majorly the spherical particles are identified but in the exposed coatings, primarily the accumulated splats were observed and a few flattened particles with asymmetrical morphology were noticed by SEM. After electrochemical corrosion testing, the EDX examination clarifies the existence of Ca, P, O, and Sr constituents in the samples being examined, and no supplementary material was found. The Ca/P ratio for HA, as well as HA-reinforced, coated samples are 1.72, 1.71, 1.68, and 1.67, respectively, indicated that the Ca/P ratio drops after dipping. It was analyzed that the concentration of oxygen in HA, HA + 4%Sr, HA + 8%Sr, and HA + 12%Sr coatings increased from 70.01%, 67.82%, 65.75% and 63.37% to 70.22%, 67.94%, 65.81%, and 63.45%, respectively, after immersion. Accordingly, it has been confirmed in prior studies that the oxygen content rises, and the Ca/P ratio reduces after immersion in Ringer's solution/simulated body fluid (Ref 67, 68). The rise in the coating's oxygen rate may also results in better bio molecular bonding to the bio-implant (Ref 69). The measurements of SEM /EDX reflect that distribution of the coating was uniform and retained morphological consistency on the addition of Sr, and the collective outcomes ensure the improved corrosion resistance of AZ31 alloy.

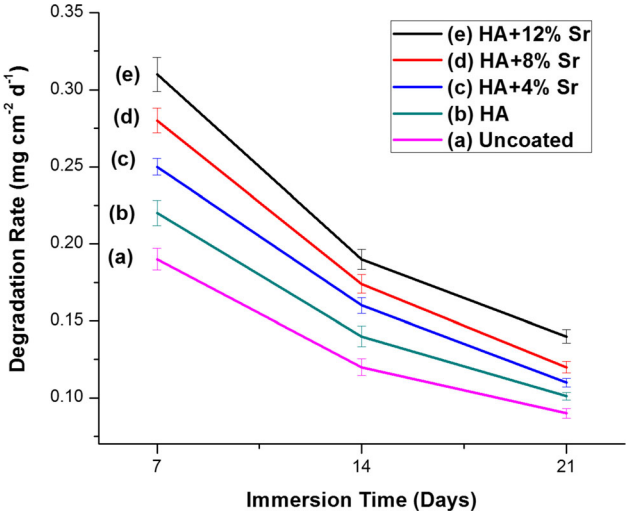

Fig. 12 Degradation rate of samples after immersion in Ringer's solution

3.3 Immersion Test

The immersion tests were performed to verify the weight loss of all the substrates. The weight loss was measured by analyzing the substrates prior to dipping and measuring the corrosion agents for 7, 14, and 21 days. The degradation rate and visual semblance of the different substrates over an immersion period of 21 days as shown in Fig. 12 and 13. The degradation rate of bare alloy observed to be extremely high for the first week because of the presence of a large concentration of Mg^{2+} ions in SBF (Ref 70). The weight loss drop was observed over the next 14 days compared to the earlier 7 days, due to the accumulation of corrosion particles on the bare substrate (Ref 71). As discussed in the earlier research, severe corrosion arises during the initial exposure phase due to the large surface area of the substrate was accessible (Ref 72). The weight loss observed for the uncoated substrate was 0.098 mg cm^{-2} d^{-1} upon 21 days of exposure, relative to all the coated substrates. The uncoated alloy showed major deterioration as observed in Fig. 13(a) (Ref 73). Due to their superior corrosion resistance, the coated samples retain their integrity in comparison to bare alloy. In Fig 13, minor corrosion cavities as well as lesser defects were found on the surface of the coated substrates. The weight loss rate of HA + 12%Sr-coated sample (0.15 mg cm^{-2} d^{-1}) during 21 days immersion was smaller than that of all coatings. Therefore, the results indicate that the modification of Sr in hydroxyapatite provides excellent corrosion resistance for the Mg substrate and enhances the life of the implant.

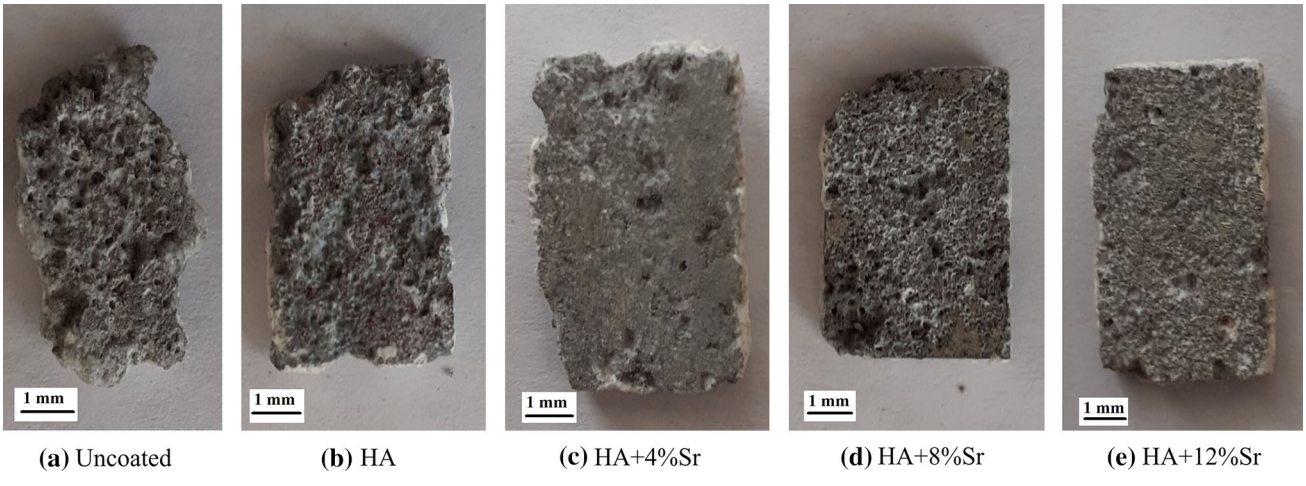

Fig. 13 Visual appearance of the corroded samples after 21 days of immersion in Ringer's solution

4. Conclusion

Plasma-sprayed coatings were successfully utilized to deposit hydroxyapatite and hydroxyapatite-strontium reinforced coatings on the AZ31 substrate. It was observed that with the rise of Sr reinforcement in HA, there was progressive increase in microhardness. HA + 12%Sr-coated sample delivered the maximum hardness value, whereas the lowest value was attained by pure HA-coated sample. On the other hands, the surface roughness is continued to decrease with Sr addition. HA + 12%Sr sample attained minimal surface roughness than all coated substrates. The SEM micrographs revealed that on all the coated samples, no microcracks were noticed, and a uniform coating thickness was obtained for all coatings reveal AZ31 substrate as a promising material for bio-implant applications. All the coated samples revealed hydrophilic properties, while the bare AZ31 alloy had hydrophobic properties. The electrochemical study showed that HA + 12%Sr-coated substrate possesses higher corrosion resistance than bare and all other coated AZ31 substrates. It was observed that with the increase in Sr reinforcement, the substrate tends to be more protective in the biological environment.

In summary, the HA/Sr coatings could be a promising strategy to enhance the surface properties, as well as the corrosion resistance of Mg implants, and thus, they deserve further biological evaluation to ascertain their usefulness for clinical applications. The obtained electrochemical as well as morphological investigations justify the potential of HA/Sr reinforced coatings for biomedical implants. The forthcoming stage of research will be focused on the in-depth phase and structural characterization of HA/Sr coatings.

Acknowledgments

The authors thankfully acknowledge Mechanical Engineering Dept., IIT Ropar, India, and Thapar Institute of Engineering and Technology, Patiala, India for providing experimental facilities and surface analysis.

Conflict of interest

The authors declare that they have no conflict of interest.

References

1. S. Gnanavel, S. Ponnusamy, L. Mohan, R. Radhika, C. Muthamizhchelvan and K. Ramasubramanian, Electrochemical Behavior of Biomedical Titanium Alloys Coated with Diamond Carbon in Hanks' Solution, *J. Mater. Eng. Perform.*, 2018, **27**, p 1635–1641
2. A.B. Elshalakany, S. Ali, A.A. Mata, A.K. Eessaa, P. Mohan, T.A. Osman and V.A. Borras, Microstructure and Mechanical Properties of Ti-Mo-Zr-Cr Biomedical Alloys by Powder Metallurgy, *J. Mater. Eng. Perform.*, 2017, **26**, p 1262–1271
3. N.S. Manam, W.S.W. Harun, D.N.A. Shri, S.A.C. Ghani, T. Kurniawan, M.H. Ismail and M.H.I. Ibrahim, Study of Corrosion in Biocompatible Metals for Implants: A Review, *J. Alloy. Compd.*, 2017, **701**, p 698–715
4. S. Bose and S. Tarafder, Calcium Phosphate Ceramic Systems in Growth Factor and Drug Delivery for Bone Tissue Engineering: A Review, *Acta. Biomater.*, 2012, **8**, p 1401–1421
5. M. Geetha, A.K. Singh, R. Asokamani and A.K. Gogia, Ti Based Biomaterials, the Ultimate Choice for Orthopaedic Implants: A Review, *Prog. Mater. Sci.*, 2009, **54**, p 397–425
6. M.A. Hussein, M. Azeem, A.M. Kumar, N. Al-Aqeeli, N.K. Ankah and A.A. Sorour, Influence of Thermal Treatment on the Microstructure, Mechanical Properties, and Corrosion Resistance of Newly Developed Ti20Nb13Zr Biomedical Alloy in a Simulated Body Environment, *J. Mater. Eng. Perform.*, 2019, **28**, p 1337–1349
7. Y. Sasikumar, A.M. Kumar, R.S. Babu, P. Dhaiveegan, N.A. Aqeeli and A.L.F. Barros, Fabrication of Brushite Coating on AZ91D and AZ31 Alloys by Two-Step Chemical Treatment and Its Surface Protection in Simulated Body Fluid, *J. Mater. Eng. Perform.*, 2019, **28**, p 3803–3815
8. Z. Cui, W. Li, L. Cheng, D. Gong, W. Cheng and W. Wang, Effect of Nano-HA Content on the Mechanical Properties, Degradation and Biocompatible Behavior of Mg-Zn/HA Composite Prepared by Spark Plasma Sintering, *Mater. Charact.*, 2019, **151**, p 620–631
9. E.S. Bogyaa, Z. Karoly and R. Barabasd, Atmospheric Plasma Sprayed Silica–Hydroxyapatite Coatings on Magnesium Alloy Substrates, *Ceram. Int.*, 2015, **41**, p 6005–6012
10. I.S. Roncevic, Z. Grubac and M.M. Hukovic, Electrodeposition of Hydroxyapatite Coating on AZ91D Alloy for Biodegradable Implant Application, *Int. J. Electrochem. Sci.*, 2014, **9**, p 5907–5923
11. Y.L. Gao, Y. Liu and X.Y. Song, Plasma-Sprayed Hydroxyapatite Coating for Improved Corrosion Resistance and Bioactivity of Magnesium Alloy, *J. Therm. Spray Technol.*, 2018, **27**, p 1–7
12. M. Supovan, Substituted Hydroxyapatites for Biomedical Applications: A Review, *Ceram. Int.*, 2015, **41**, p 9203–9231
13. S. Zhou, Y. Bai, W. Ma and W. Chen, Suspension Plasma-Sprayed Fluoridated Hydroxyapatite/Calcium Silicate Composite Coatings for Biomedical Applications, *J. Therm. Spray Technol.*, 2019, **28**, p 1025–1038
14. N. Bosh, H.M. Jovein and C. Muller, Determination of Triaxial Residual Stress in Plasma-Sprayed Hydroxyapatite (HAp) Deposited on Titanium Substrate by X-ray Diffraction, *J. Therm. Spray Technol.*, 2018, **27**, p 1–13
15. M. Ohki, S. Takahashi, R. Jinnai and T. Hoshina, Interfacial Strength of Plasma-sprayed Hydroxyapatite Coatings, *J. Therm. Spray Technol.*, 2020, **29**, p 1119–1133
16. V. Deram, C. Minichiello, R.N. Vannier, A.L. Maguer, L. Pawlowski and D. Murano, Microstructural Characterizations of Plasma Sprayed Hydroxyapatite Coatings, *Surf. Coat. Technol.*, 2003, **166**, p 153–159
17. M. Ramadas, G. Bharath, N. Ponpandian and A.M. Ballamurugan, Investigation on Biophysical Properties of Hydroxyapatite/Graphene Oxide (HAp/GO) Based Binary Nanocomposite for Biomedical Applications, *Mater. Chem. Phys.*, 2017, **199**, p 179–184
18. S. Dyshlovenko, C. Pierlot, L. Pawlowski, R. Tomaszek and P. Chagnon, Experimental Design of Plasma Spraying and Laser Treatment of Hydroxyapatite Coatings, *Surf. Coat. Technol.*, 2006, **201**, p 2054–2060
19. Y. Sasikumar, M. Karthega and N. Rajendran, In Vitro Bioactivity of Surface-Modified β-Ti Alloy for Biomedical Applications, *J. Mater. Eng. Perform.*, 2011, **20**, p 1271–1277
20. B. Moore, E. Asadi and G. Lewis, Deposition Methods for Microstructured and Nanostructured Coatings on Metallic Bone Implants: A Review, *Adv. Mater. Sci. Eng.*, 2017, **2017**, p 1–9
21. P. Gkomoza, M. Vardavoulias, D.I. Pantelis and C. Sarafoglou, Comparative Study of Structure and Properties of Thermal Spray Coatings Using Conventional and Nanostructured Hydroxyapatite Powder, for Applications in Medical Implants, *Surf. Coat. Technol.*, 2019, **357**, p 748–758
22. R. Kumari and J.D. Majumdar, Heat-Treated TiO_2 Plasma Spray Deposition for Bioactivity Improvement in Ti-6Al-4V Alloy, *J. Mater. Eng. Perform.*, 2017, **26**, p 6207–6218
23. Y.C. Yang and C.Y. Yang, Mechanical and Histological Evaluation of a Plasma Sprayed Hydroxyapatite Coating on a Titanium Bond Coat, *Ceram. Int.*, 2013, **39**, p 6509–6516
24. R.B. Heimann, Plasma-Sprayed Hydroxylapatite-Based Coatings: Chemical, Mechanical, Microstructural, and Biomedical Properties, *J. Therm. Spray Technol.*, 2016, **25**, p 827–850
25. A. Srinivasan and N. Rajendran, Electrochemical Corrosion and In Vitro Bioactivity of SiO_2:ZrO_2-Coated 316L Stainless Steel in Simulated Body Fluid, *J. Mater. Eng. Perform.*, 2015, **24**, p 3056–3067
26. K. Li, J. Yu, Y. Xie, L. Huang, X. Ye and X. Zheng, Effects of Zn Content on Crystal Structure, Cytocompatibility, Antibacterial Activity, and Chemical Stability in Zn-Modified Calcium Silicate Coatings, *J. Therm. Spray Technol.*, 2013, **22**, p 1–9

27. Y. Li, X. Shui, L. Zhang and J. Hu, Cancellous Bone Healing Around Strontium-Doped Hydroxyapatite in Osteoporotic Rats Previously Treated with Zoledronic Acid, *J. Biomed. Mater. Res. B*, 2015, **104**, p 476–481
28. J.H. Shepherd and D.V. Shepherd, Best, Substituted Hydroxyapatites for Bone Repair, *J. Mater. Sci. Mater. Med.*, 2012, **23**, p 2335–2347
29. L. Xu, E. Zhang, D. Yin, S. Zeng and K. Yang, In Vitro Corrosion Behavior of Mg Alloys in a Phosphate Buffered Solution for Bone Implant Application, *J. Mater. Sci. Mater. Med.*, 2008, **19**, p 1017–1025
30. A.R. Boyd, L. Rutledge, L.D. Randolph and B.J. Meenan, Strontium-Substituted Hydroxyapatite Coatings Deposited Via a Co-deposition Sputter Technique, *Mater. Sci. Eng. C*, 2015, **46**, p 290–300
31. D. Gopi, A. Karthika, D. Rajeswari, L. Kavitha, R. Pramod and J. Dwivedi, Investigation on Corrosion Protection and Mechanical Performance of Minerals Substituted Hydroxyapatite Coating on HELCDEB-Treated Titanium Using Pulsed Electrodeposition Method, *RSC Adv.*, 2014, **66**, p 34751–34759
32. K. Ozeki, T. Goto, H. Aoki and T. Masuzawa, Characterization of Sr-Substituted Hydroxyapatite Thin Film by Sputtering Technique from Mixture Targets of Hydroxyapatite and Strontium Apatite, *Bio Med. Mater. Eng.*, 2014, **24**, p 1447–1456
33. H.S. Fekri, M. Ranjbar, G.D. Noudeh and N. Ziasistani, Green Synthesis of Strontium Nanoparticles Self-assembled in the Presence of Carboxymethyl Cellulose: An In Vivo Imaging Study, *J. Bio. Chem. Lumin.*, 2019, **34**, p 1–7
34. R.B. Heimann, Plasma-Sprayed Hydroxylapatite Coatings as Biocompatible Intermediaries Between Inorganic Implant Surfaces and Living Tissue, *J. Therm. Spray Technol.*, 2018, **27**, p 1212–1237
35. A. Singh, G. Singh and V. Chawla, Characterization and Mechanical Behaviour of Reinforced Hydroxyapatite Coatings Deposited by Vacuum Plasma Spray on SS-316L Alloy, *J. Mech. Behav. Biomed. Mater.*, 2018, **79**, p 273–282
36. A.R. Kmita, A. Slosarczyk, Z. Paszkiewicz and D. Paluch, Evaluation of HAp-ZrO2 Composites and Monophase Hap Bioceramics. Vitro Study, *J. Mater. Sci.*, 2004, **39**, p 5865–5867
37. J.E. Tercero, S. Namin, D. Lahiri, K. Balani, N. Tsoukias and A. Agarwal, Effect of Carbon Nanotube and Aluminum Oxide Addition on Plasma-Sprayed Hydroxyapatite Coating's Mechanical Properties and Biocompatibility, *Mater. Sci. Eng. C*, 2009, **29**, p 2195–2202
38. L. Sun, C.C. Berndt, K.A. Gross and A. Kucuk, Material Fundamentals and Clinical Performance of Plasma-Sprayed Hydroxyapatite Coatings: A Review, *J. Biomed. Mater. Res.*, 2001, **58**, p 570–592
39. M. Shaban, F. Mohamed and S. Abdallah, Production and Characterization of Superhydrophobic and Antibacterial Coated Fabrics Utilizing ZnO Nanocatalyst, *Sci. Rep.*, 2018, **8**, p 3925–3940
40. L.G. Ellies, D.G.A. Nelson and J.D.B. Featherstone, Crystallographic Changes in Calcium Phosphates During Plasmaspraying, *Biomaterials*, 1992, **13**, p 313–316
41. B. Singh, G. Singh and B.S. Sidhu, Investigation of the In Vitro Corrosion Behavior and Biocompatibility of Niobium (Nb)-Reinforced Hydroxyapatite (HA) Coating on CoCr Alloy for Medical Implants, *J. Mater. Res.*, 2019, **34**, p 1678–1691
42. M. Roy, A. Bandyopadhyay and S. Bose, Induction Plasma Sprayed Sr and Mg Doped Nano Hydroxyapatite Coatings on Ti for Bone Implant, *J Biomed. Mater. Res. B Appl. Biomater*, 2011, **99**, p 258–265
43. B. Singh, G. Singh and B.S. Sidhu, Analysis of Corrosion Behaviour and Surface Properties of Plasma-Sprayed Composite Coating of Hydroxyapatite–Tantalum on Biodegradable Mg Alloy ZK60, *J. Compos. Mater.*, 2019, **53**, p 2661–2673
44. C.W. Kang and F.Z. Fang, State of the Art of Bioimplants Manufacturing, *Adv. Manuf.*, 2018, **6**, p 20–40
45. G. Singh, S. Singh and S. Prakash, Surface Characterization of Plasma Sprayed Pure and Reinforced Hydroxyapatite Coating on Ti6Al4V Alloy, *Surf. Coat. Technol.*, 2011, **205**, p 4814–4820
46. B. Singh, G. Singh and B.S. Sidhu, Analysis of Corrosion Behavior and Surface Properties of Plasma-Sprayed HA/Ta Coating on CoCr Alloy, *J. Therm. Spray Technol.*, 2018, **27**, p 1401–1413
47. X. Zhao, C. Peng and J. You, Plasma-Sprayed ZnO/TiO_2 Coatings with Enhanced Biological Performance, *J. Therm. Spray Technol.*, 2017, **26**, p 1301–1308
48. D. Yamashita, M. Machigashira, M. Miyamoto, H. Takeuchi, K. Noguchi, Y. Izumi and S. Ban, Effect of Surface Roughness on Initial Responses of Osteoblast-Like Cells on Two Types of Zirconia, *Dent. Mater. J.*, 2009, **28**, p 461–470
49. F.A. Shah, M.L. Johansson, O. Omar, H. Simonsson, A. Palmquist and P. Thomsen, Laser-Modified Surface Enhances Osseointegration and Biomechanical Anchorage of Commercially Pure Titanium Implants for Bone-Anchored Hearing Systems, *PLoS ONE*, 2016, **11**, p 1–24
50. K.A. Gross and M. Babovic, Influence of Abrasion on the Surface Characteristics of Thermally Sprayed Hydroxyapatite Coatings, *Biomaterals.*, 2002, **23**, p 4731–4737
51. W. Wang, G. Caetano, W.S. Ambler, J.J. Blaker, M.A. Frade, P. Mandal, C. Diver and P. Bartolo, Enhancing the Hydrophilicity and Cell Attachment of 3D Printed PCL/Graphene Scaffolds for Bone Tissue Engineering, *Materials*, 2016, **992**, p 1–11
52. S. Durdu, K. Korkmaz, S.L. Aktug and A. Cakir, Characterization and Bioactivity of Hydroxyapatite-Based Coatings Formed on Steel by Electro-Spark Deposition and Micro-Arc Oxidation, *Surf. Coat. Technol.*, 2017, **326**, p 1–41
53. B. Houa, Y. Liua, H. Chena and Y. Yanga, In vitro Bioactivity, Bio-Corrosion Resistance and Antibacterial Property of Laser Cladded HA Coatings with Different Content of ZnO on Ti-6Al-4V Substrate, *Mater. Res.*, 2019, **22**, p 1–10
54. M. Sankar, S. Suwas, S. Balasubramanian and G. Manivasagam, Comparison of Electrochemical Behavior of Hydroxyapatite Coated onto WE43 Mg Alloy by Electrophoretic and Pulsed Laser Deposition, *Surf. Coat. Technol.*, 2017, **309**, p 840–848
55. T.P.S. Sarao, H. Singh and H. Singh, Enhancing Biocompatibility and Corrosion Resistance of Ti-6Al-4V Alloy by Surface Modification Route, *J. Therm. Spray Technol.*, 2018, **27**, p 1388–1400
56. S. Stojadinovic, N. Tadic, N. Radic, B. Grbic and R. Vasilic, MgO/ZnO Coatings Formed on Magnesium Alloy AZ31 by Plasma Electrolytic Oxidation: Structural, Photoluminescence and Photocatalytic Investigation, *Surf. Coat. Technol.*, 2017, **310**, p 98–105
57. J. Kim, H.M. Mousa, C.H. Park and C.S. Kim, Enhanced Corrosion Resistance and Biocompatibility of AZ31 Mg Alloy Using PCL/ZnO NPs via Electrospinning, *Appl. Surf. Sci.*, 2017, **396**, p 249–258
58. M.H. Fathi and F. Azam, Novel Hydroxyapatite/Tantalum Surface Coating for Metallic Dental Implant, *Mater. Lett.*, 2007, **61**, p 1238–1241
59. G. Singh, H. Singh and B.S. Sidhu, Corrosion Behavior of Plasma Sprayed Hydroxyapatite and Hydroxyapatite-Silicon Oxide Coatings on AISI, 304 for Biomedical Application, *Appl. Surf. Sci.*, 2013, **284**, p 811–818
60. S. Dudin, C.M. Cotrut, M. Dinu, A. Zykova, A.C. Parau, S. Yakovin and A. Vladescu, Comparative Study of the Hydroxyapatite Coatings Prepared with/Without Substrate Bias, *Ceram. Int.*, 2017, **43**, p 14968–14975
61. R. Walter and M.B. Kannan, Influence of Surface Roughness on the Corrosion Behaviour of Magnesium Alloy, *Mater. Des.*, 2011, **32**, p 2350–2354
62. M.F. Hasan, J. Wang and C. Berndt, Determination of the Mechanical Properties of Plasma-Sprayed Hydroxyapatite Coatings Using the Knoop Indentation Technique, *J. Therm. Spray Technol.*, 2015, **24**, p 865–877
63. J. Feng, Y. Chen, X. Liu, T. Liu, L. Zou, Y. Wang, Y. Ren, Z. Fan, Y. Lv and M. Zhang, Insitu Hydrothermal Crystallization $Mg(OH)_2$ Films on Magnesium Alloy AZ91 and Their Corrosion Resistance Properties, *Mater. Chem. Phys.*, 2013, **143**, p 322–329
64. S. Durdu, S.L. Aktug and K. Korkmaz, Characterization and Mechanical Properties of the Duplex Coatings Produced on Steel by Electro-spark Deposition and Micro-arc Oxidation, *Surf. Coat. Technol.*, 2013, **236**, p 303–308
65. S. Mohajernia, S.P. Ali, S. Hejazi, M. Saremi and A.R.K. Rashid, Hydroxyapatite Coating Containing Multi-walled Carbon Nanotubes on AZ31 Magnesium: Mechanical-Electrochemical Degradation in a Physiological Environment, *Ceram. Int.*, 2018, **44**, p 8297–8305
66. K.A. Hing, I.R. Gibson, P.A. Revell, S.M. Best and W. Bonfield, Influence of Phase Purity on the In Vivo Response to Hyrdoxyapatite, *Key Eng. Mater.*, 2001, **373**, p 192–195
67. G.L. Burke, The Corrosion of Metals in Tissues; and an Introduction to Tantalum, *Can. Med. Assoc. J.*, 1940, **43**, p 125–128
68. Z. Zhang, M.F. Dunn, T.D. Xiao, A.P. Tomsia and E. Saiz, Nanostructured Hydroxyapatite Coatings for Improved Adhesion and Corrosion Resistance for Medical Implants, *Mater. Res. Soc. Symp. Proc.*, 2002, **703**, p 291–297

69. H. Wang, Y. Zheng, C. Jiang, Y. Li and Y. Fu, In Vitro Corrosion Behavior and Cytocompatibility of Pure Fe Implanted with Ta, *Surf. Coat. Technol.*, 2017, **320**, p 201–206
70. M. Jamesh, S. Kumar and T.S.N.S. Narayanan, Corrosion Behavior of Commercially Pure Mg and ZM21 Mg Alloy in Ringer's Solution–Long Term Evaluation by EIS, *Corros. Sci.*, 2011, **53**, p 645–654
71. F. Geng, L.L. Tan, X.X. Jin, J.Y. Yang and K. Yang, The Preparation, Cytocompatibility, and In Vitro Biodegradation Study of Pure β-TCP on Magnesium, *J. Mater. Sci. Mater. Med.*, 2009, **20**, p 1149–1157
72. X.N. Gu, S.S. Li, X.M. Li and Y.B. Fan, Magnesium Based Degradable Biomaterials: A Review, *Front. Mater. Sci.*, 2014, **8**, p 200–218
73. Y. Xin, C. Liu, X. Zhang, G. Tang, X. Tian and P.K. Chu, Corrosion Behavior of Biomedical AZ91 Magnesium Alloy in Simulated Body Fluids, *J. Mater. Res.*, 2007, **22**, p 2004–2011